https://doi.org/10.5194/egusphere-2026-4469
Preprint. Discussion started: 7 August 2026

Deriving Subsurface Stormflow Mechanisms with Isotopes and ERT

Jonas Pyschik[1], Veronica Cordero[1], Jakob Wilk[1], Veronika Lechner[2], Emanuel Thoenes[3], Stefan Achleitner[3], Bernhard Kohl[2], Markus Weiler[1], and Stefan Hergarten[1]

[1]Institute of Earth and Environmental Sciences, Universität Freiburg, Germany
[2]Austrian Research Centre for Forests (BFW), Innsbruck, 6020, Austria
[3]Unit of Hydraulic Engineering, Department of Infrastructure, University of Innsbruck, Innsbruck, 6020, Austria

Correspondence: Jonas Pyschik (jonas.pyschik@geologie.uni-freiburg.de) and Veronica Cordero (veronica.cordero@geologie.uni-freiburg.de)

Abstract.

Subsurface stormflow (SSF) is a dominant process in the generation of runoff in many catchments. However, the mechanisms by which new event water triggers the activation and release of stored pre-event water are not well understood. To identify the flow paths and mechanisms governing SSF generation, we conducted a controlled sprinkling experiment using deuterium-labeled water alongside time-lapse electrical resistivity tomography (ERT), groundwater monitoring and soil core sampling at two trenched hillslopes in the Black Forest, Germany. Water was applied for three hours, with the supply switching to deuterated water halfway through the experiment. Both hillslopes responded rapidly, with event runoff coefficients of approximately 0.6, and tracer breakthrough occurred at the trenches within 7–18 minutes of application, even at depths greater than 70 cm. However, post-irrigation soil cores detected the tracer only in the uppermost 20 cm of the soil matrix, where approximately 45 % of the labeled water remained stored. Time-lapse ERT revealed that the wetting front was largely confined to the upper 0.2–1.5 m; meanwhile, the deeper, near-saturated zone exhibited negligible resistivity change despite sustained lateral discharge as measured at the trenches.

Together, these observations suggest the presence of a dual-domain flow system, whereby a small proportion of event water bypasses the matrix via vertically and laterally connected preferential pathways. Meanwhile, the majority of SSF consists of pre-event water, which is mobilized by pressure-driven (piston) displacement within the saturated zone. Subsequent natural rainfall remobilized the stored tracer, raising the cumulative recovery rate to approximately 30 % within one month, thereby confirming the soil matrix to be both a sink and a delayed source of event water.

1 Introduction

Subsurface stormflow (SSF) refers to the lateral movement of water through hillslope soils above a less permeable layer, such as bedrock or a less vertically conductive soil horizon (Weiler et al., 2005; Chifflard et al., 2019; McGuire et al., 2024). This process is a key runoff generation mechanism, particularly in sloped, structured soils. SSF has been documented across a wide range of biomes, excluding deserts, but it is most prevalent in humid, temperate environments where permeable soils and

https://doi.org/10.5194/egusphere-2026-4469
Preprint. Discussion started: 7 August 2026

sufficient precipitation sustain it (McMillan et al., 2025). In such settings, SSF can account for up to 90 % of total rainfall volume (Beasley, 1976).

SSF initiates rapidly in response to precipitation or snowmelt and can occur even under relatively dry antecedent soil conditions (Beasley, 1976; Kelln et al., 2007). However, SSF generation is threshold-dependent, requiring a minimum precipitation volume or intensity which must first be exceeded before it occurs. After this threshold is reached, flow rates increase rapidly (Tromp-van Meerveld and McDonnell, 2006).

SSF is commonly conceptualized in terms of two main flow domains: lateral matrix flow and preferential flow. Lateral matrix flow refers to the downslope transmission of water and commonly develops where infiltrating water accumulates above a low-conductivity soil layer or the soil-bedrock interface, which then drains slowly laterally through the soil pore space (Weiler et al., 2005). Preferential flow occurs through connected flow networks, such as connected macropores and soil pipes, which can span entire slopes and transmit water much faster than the surrounding matrix (Guo et al., 2014; Anderson et al., 2009b; Wilson et al., 2016; Angermann et al., 2017). These preferential pathways largely account for the rapid runoff responses (Anderson et al., 2009b; Beven and Germann, 2013; Angermann et al., 2017).

Tracers are widely used to study SSF generation, flow dynamics, and source areas. Stable water isotopes are a particularly powerful tool for this study. By distinguishing between pre-event and event water, isotopes can reveal travel times, mixing processes, and the contribution of preferential flow pathways to SSF (Newman et al., 1998; van Verseveld et al., 2017). Although preferential pathways rapidly transmit young event water deep into the soil, bypassing older water stored in the matrix (Gazis and Feng, 2004; Peralta-Tapia et al., 2015), the bulk of SSF typically consists of older, pre-event water (Anderson et al., 2009b; van Verseveld et al., 2017; Rinderer et al., 2021). This "old water paradox" underscores the value of isotopic tracers in distinguishing the fast and slow flow mechanisms that drive subsurface runoff generation (McDonnell, 1990).

However, applying isotopic tracers under natural rainfall is difficult for two reasons. First, the input signal is difficult to constrain. Canopy interception enriches throughfall with heavy isotopes compared to bulk precipitation. Furthermore, throughfall composition varies substantially over short distances (Brodersen et al., 2000; Kato et al., 2013; Allen et al., 2015), which makes defining a representative input for mixing models difficult. Second, natural storms activate source areas unevenly across the hillslope. Zones with low storage thresholds contribute to SSF early on, while areas with greater storage capacity remain hydrologically disconnected (Hopp and McDonnell, 2009; Fujimoto et al., 2011). SSF generation therefore depends not only on rainfall volume, but also on how saturated zones connect in space and time.

Controlled irrigation experiments address these uncertainties directly. Sprinkling induces SSF reproducibly and within a spatially constrained domain by applying a known volume of water with a defined isotopic signature over a specified upslope area. This eliminates the confounding effects of throughfall variability and uncontrolled source area activation. (Angermann et al., 2017; van Verseveld et al., 2017; Scaini et al., 2017; Rinderer et al., 2021).

Direct observation of SSF pathways remains challenging for both natural as well as sprinkling induced SSF events. Flow presumably occurs along easily disturbed, heterogeneous and transient subsurface pathways that are difficult to monitor using standardized hydrological methods. Electrical Resistivity Tomography (ERT) therefore has become an important tool for investigating hillslope hydrological processes and is already well-established for tracing water infiltration and imaging tracer

https://doi.org/10.5194/egusphere-2026-4469
Preprint. Discussion started: 7 August 2026

progression (Scaini et al., 2017). The sensitivity of electrical resistivity to water content and pore-water conductivity allows non-invasive imaging of dynamic processes like infiltration and subsurface flow.

Early applications demonstrated the potential of ERT to identify hydrological process areas and preferential groundwater flow paths on hillslopes. Koch (2004) combined ERT with tracer observations to delineate saturated zones and subsurface hydraulic connections within a hillslope–floodplain system in the Black Forest, Germany, highlighting the ability of ERT to reveal hydrologically active structures that are difficult to identify from point measurements alone. Uhlenbrook and Wenninger (2006) used ERT to identify hillslope flow pathways and emphasized its value for visualizing subsurface connectivity relevant to runoff generation. Leslie and Heinse (2013) applied pseudo-three-dimensional ERT to characterize soil-pipe networks on forested hillslopes, demonstrating the capability of resistivity imaging to detect preferential flow structures that can rapidly transmit water downslope.

Despite these advances, the interpretation of ERT data during active infiltration experiments remains challenging. Resistivity reductions caused by infiltrating water are often dominated by near-surface processes, making it difficult to distinguish vertical infiltration from lateral subsurface stormflow. Furthermore, the inherently three-dimensional nature of hillslope flow can violate the assumptions underlying two-dimensional inversions and introduce artifacts into interpreted resistivity models. Consequently, while ERT has proven valuable for identifying hydrologically relevant structures and monitoring moisture redistribution, its ability to separately resolve vertical and lateral flow components, in particular during controlled rainfall experiments, remains insufficiently constrained.

Isotopic tracers and ERT offer complementary views of SSF. Tracers distinguish between pre-event and event water, but they cannot identify where flow occurs. ERT images subsurface structure and wetting, but distinguishing vertical infiltration from lateral flow on basis of ERT data alone remains challenging. Combining the two methods provides a means of constraining the sources and flow paths of SSF. This is important because previous studies consistently show that SSF is predominantly composed of pre-event water, despite the input of new event water during precipitation (Anderson et al., 2009b; van Verseveld et al., 2017; Rinderer et al., 2021). However, the mechanisms by which new rainfall triggers the release of this stored water remain poorly understood. To address this gap, we pose three questions: How and where does new event water contribute to SSF? What are the dominant flow paths? And how can isotopic tracers and ERT jointly characterize subsurface flow dynamics?

We address these questions through a controlled, tracer-based sprinkling experiment combined with ERT. This approach lets us track labeled event water as it moves through the hillslope, and gives insights of where it is stored and transported before it is ultimately discharged.

2 Methods

2.1 Study Site

The study was conducted in the Ruetlidobel catchment and the neighboring Eberbach catchment (Appendix Figure A1), which are located on the western edge of the Black Forest in south-western Germany, near Freiburg im Breisgau (47°57’20.6"N, 7°50’23.2"E). These headwater catchments cover a total area of 1.81 km^2 and span an elevation range of 340–585 m above

https://doi.org/10.5194/egusphere-2026-4469
Preprint. Discussion started: 7 August 2026

sea level. Due to extensive previous research, the area is well established as a site for studying hillslope hydrology and lateral subsurface flow processes (Bachmair and Weiler, 2012; Pyschik et al., 2025a; Thoenes et al., 2026a).

The landscape is characterized by a mosaic of grasslands, mixed forests and coniferous forests. The region has a temperate humid climate with an average annual rainfall of around 970 mm and an average annual temperature of 11 °C. Rainfall exhibits clear seasonal contrasts. Summer precipitation is often associated with short-duration, high-intensity convective storms, whereas winter rainfall typically occurs as longer-lasting, lower-intensity precipitation. Cambisols have developed on periglacial drift deposits that cover the underlying bedrock, creating pronounced vertical and lateral heterogeneity in hydraulic properties.

To investigate lateral subsurface flow processes, three trenches were installed on hillslopes that differ in terms of gradient, aspect, land use and geomorphic form. The trenches are located within 20 meters of the adjacent streams. This study focuses on two forested trenches, referred to as Trench 1 and Trench 3.

Trench 1 is located on a northwest-facing hillslope with a mean slope angle of 18.5° and planar form. The vegetation consists of a mixed forest dominated by Hornbeam (*Carpinus betulus*) and Spruce (*Picea abies*), with a sparse understorey. The subsurface profile comprises periglacial drift deposits. Above Trench 1 (approximately one quarter of the trench length from the right-hand, SW-facing edge), a small spring emerges, resulting in elevated soil water contents in the underlying profile. In this section of the trench, the typical Bv horizon is replaced by a grayish, reduced Gr horizon which in the middle of the Trench is overlain by a thin rust-colored Go horizon (Figure 1a).

Trench 3 is located on a steeper, southwest-facing hillside with an average slope angle of 26.6° and an convex-convergent shape. The area is dominated by coniferous forest, primarily consisting of Hornbeam (*Carpinus betulus*) and Fir (*Abies alba*). The subsurface exhibits pronounced periglacial characteristics, notably the presence of coarse rock fragments dispersed throughout the soil profile but most present in the upper 0.4-0.6 m below ground level. Bedrock was encountered during excavation and installation on the east side of the Trench (Figure 1b).

2.2 Data Collection

2.2.1 SSF Trenches

The trenches were installed perpendicular to the hillslope in order to intercept and quantify lateral SSF (Figure 2). Each trench was 11–15 meters long and was excavated to bedrock or to a depth of approximately 2–3 meters. Along the exposed soil face, drainage mats were installed. These mats consisted of a rigid, dimpled plastic core covered by a geotextile facing the soil. The mats intercepted lateral flow and directed it downward within the mat structure. Perforated drainage pipes were installed beneath each mat to collect the intercepted water. The pipes were partially encased in pond liner to prevent leakage and ensure complete capture of the flow deflected by the mats. All pipes were installed with a slight downslope gradient to enable gravity-driven flow, and were connected to solid tubing which routed the water outside the hillslope to measurement stations. To distinguish between SSF depth contributions, each trench was divided into two collection layers (Top: 0.5–0.7 m and 0.4–0.6 m at Trench 1 and 3 respectively; Bottom 2.7–2.9 m and 1.2–2.1 m at Trench 1 and 3 respectively) by separating the

https://doi.org/10.5194/egusphere-2026-4469
Preprint. Discussion started: 7 August 2026

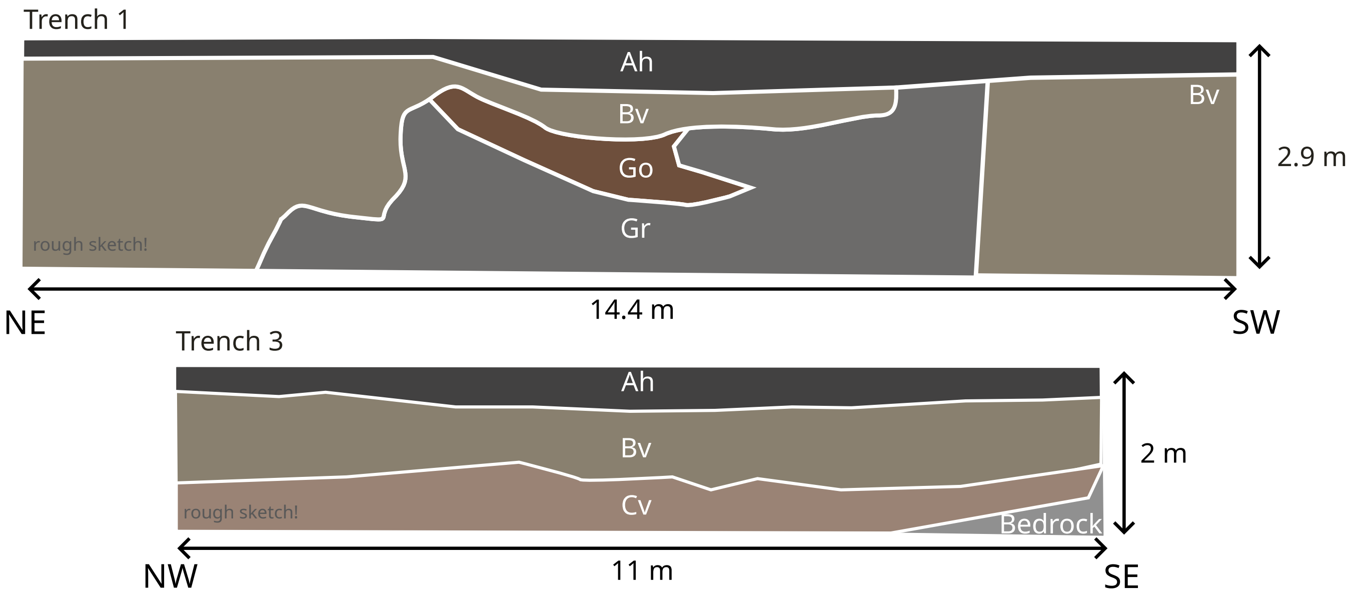

Figure 1. Rough sketch of soil description German KA5 (Sponagel et al., 2005) of Trench 1 (Gley Cambisol) and Trench 3 (Cambisol) during Trench installation. Soil Horizons are Ah = humic topsoil horizon; Bv = cambic subsurface horizon; Cv = weathered parent material; Go = oxidized gleyic horizon; Gr = reduced gleyic horizon.

drainage mat horizontally and installing a second independent pipe-liner system. After installation, the trenches were carefully backfilled. During the experiments, discharge was measured using custom-build tipping buckets for flows of up to around 300 liters per hour, while higher flowrates were quantified manually using 200-liter containers and timed volume measurements. A detailed schematic of the trench installations can be found in Pyschik et al. (2025a) and Thoenes et al. (2026a).

2.2.2 Groundwater Wells

Five groundwater monitoring wells were installed upslope from the trench to characterize the groundwater level (GWL) dynamics (Figure 2). Three of the wells were positioned approximately 2.5 to 5 meters upslope from the trench face and were aligned parallel to the trench, with roughly 5-meter spacing between them (A3-A5). Two additional wells were installed further upslope from the central well of this transect at distances of approximately 10 meters (A2) and 20 meters (A1), respectively, forming a longitudinal transect perpendicular to the trench.

All wells were drilled to refusal depth (approx. 2-3 m) using an electric jackhammer (Makita HM1810). The boreholes had a diameter of 6 cm and were equipped with perforated PVC casing wrapped in a geotextile sleeve. Each well was equipped with a water pressure sensor (Truebner) to continuously record groundwater levels.

https://doi.org/10.5194/egusphere-2026-4469
Preprint. Discussion started: 7 August 2026

2.2.3 Sprinkling Experiment

A controlled sprinkling experiment was conducted above each trench (Thoenes et al., 2026b). The irrigated plot measured 10 meters in width — narrower than the trench itself to ensure the capture of laterally mobilized flow — and 20 meters in length. Eight rotating sprinklers (Rain Bird 5000 rotor sprinklers) were positioned at the four corners and midpoints of each long side such that each sprinkler was within 10 meters of at least two neighbors to ensure even coverage. The applied water volume was recorded every 10 seconds. The average sprinkling intensity was approximately 15 - 16.6 mm h^{-1}, and the experiment ran for a total duration of three hours. Water was supplied from two mobile pools filled with stream water prior to the experiment, with one pool being labeled to approximately + 220 ‰ with deuterated water. After approximately 1.5 hours, the water source was changed to the deuterated pool.

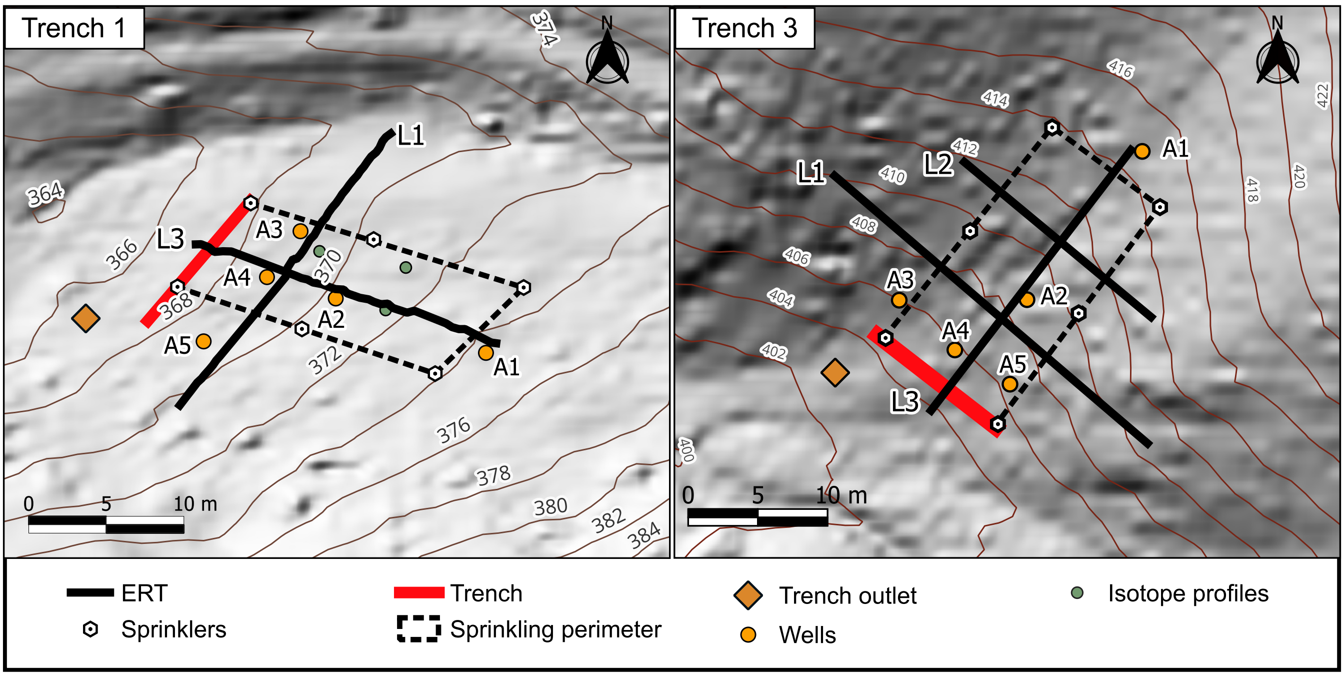

Figure 2. Sprinkling area (dashed lines) and ERT setup (black lines) for both trenches. Red lines mark the trench locations; white dots the rotor sprinklers; orange dots the groundwater wells; and green dots (Trench 1 only - one day and one month after irrigation) the isotope core-drilling locations. Map made by the authors with data from LGL BW (2026)

For Trench 1, the wells A2, A3 and A4 were within the sprinkled area, for Trench 3, the sprinkled area overlapped with A2, A4 and A5, with A3 being just outside.

https://doi.org/10.5194/egusphere-2026-4469
Preprint. Discussion started: 7 August 2026

2.2.4 Isotope Sampling

Water samples were collected at 20-minute intervals from the start of irrigation until two hours after irrigation ceased. Additionally, ISCO automatic samplers were installed, continuing to collect samples every 16 hours for one month after the experiment. All analyses of stable water isotopes were performed at the Chair of Hydrology, University of Freiburg, using a Picarro L2130-i cavity ring-down laser spectrometer, with measurement uncertainties of ± 0.04 ‰ for δ^{18}O and ± 0.26 ‰ for δ^{2}H.

To assess soil water redistribution, soil pore water was sampled at Trench 1 one day after irrigation and one month later (Figure 2). Five soil core profiles (3 and 2 after 1 day and 1 month respectively) were collected within the irrigated area, and one reference profile was collected outside of the plot. Cores were extracted to refusal depth (2-3 m) using an electric drill (Makita HM1810). To avoid contamination, the upper 5 cm of each core was discarded and samples were taken at 10–20 cm depth intervals. The samples were stored in 500 ml aluminium-laminated plastic bags (WEBER Packing GmbH, CB400-420BRZ), which were sealed using its zip-lock.

Soil water isotope ratios were determined using the direct vapor equilibration method. The bags were inflated with dry air, heat-sealed and fitted with silicone septa. They were then stored at 20 ± 1 °C for 48 hours to allow equilibration between the liquid and vapor phases. The samples' headspace vapor was analyzed with a Picarro L2130-i and VapAuSa, following the stability criteria described in Pyschik et al. (2025b). All isotope ratios were calibrated to the VSMOW-SLAP scale using in-house standards, co-measured after every 15 samples and results were reported in delta notation relative to Vienna Standard Mean Ocean Water (VSMOW) (Craig, 1961).

2.2.5 ERT

Time-lapse surface ERT surveys were carried out in both Trench 1 and Trench 3 during the sprinkling experiments. Two ERT profiles parallel to the trench and one perpendicular to it were installed across the sprinkling area, except in Trench 1, where only one parallel profile was used, as shown in Figure 2. The number of electrodes and electrode spacing varied; these are described in Table 1. The ERT instrumentation consisted of a Lippmann 4-point light 10 W resistivity meter with active electrode chains and two Syscal Pro units. The survey acquisition was performed using the Wenner-α array configuration. For each time step, a stack of 3 measurements with a 1 % error tolerance was accepted; if the tolerance was not met, 6 measurements were stacked instead.

Table 1. Summary of ERT acquisition parameters

	Trench 1		Trench 3		
	L1	L3	L1	L2	L3
Total length (m)	29.5	23.5	29.5	17.25	23.5
Number of electrodes	60	48	60	24	48
Electrode separation (m)	0.5	0.5	0.5	0.75	0.5
Measurements / cycle	570	360	570	84	360

Contact resistance was checked before irrigation to ensure it was below 10 kω. The first measurement cycle was conducted prior to the experiment to serve as a baseline (pre-sprinkling resistivity). During the sprinkling experiment, monitoring cycles including all profiles were repeated approximately every 1 h to 1:15 h; the recording time for each profile was around 15-20 minutes. Monitoring continued for up to 6 hours after the start of sprinkling, with an additional measurement after approximately 23 hours. At Trench 3, however, this additional measurement was not included in the analysis due to a natural rain event that occurred around 7 h after the sprinkling.

2.3 Data Analysis

2.3.1 Isotope Mixing Models

Bayesian mixing models were applied using the simmr package (Govan and Parnell, 2023) in R to distinguish the contributions of tracer and pre-event waters. Pre-event water was defined as the isotopic signature of the trench baseflow water sampled prior to irrigation, while the event water signature consisted of the sprinkler water from the deuterated pool. All subsequent SSF samples collected during the experiment were treated as mixtures. To align the mixing results and discharge data, the mixing results were linearly interpolated to a resolution of 10 minutes, which matched that of the SSF discharge. This allowed the estimation of the tracer fractions for each flow time step.

The mixing framework was also applied to estimate the storage of tracer water in the soil matrix at Trench 1. In this case, the background source was defined as soil water from the reference profile outside the irrigated area, the tracer source was defined as deuterated sprinkler water and the mixture was defined as the isotope composition of the top 20 cm of soil within the irrigated zone. Assuming a mean soil porosity of 0.55 (see Thoenes et al. (2026a) table 1 for soil properties of each trench) and full saturation of the 200 m^2 plot following irrigation, the total pore volume in the top 20 cm was estimated to be around 22 m^3, which provided a basis for quantifying tracer storage volume in the near-surface soil.

2.3.2 ERT Inversion

Time-lapse 2D inversions were performed to derive the subsurface electrical resistivity distribution from the measured apparent resistivity data for each ERT profile, using the PyGIMLi Library for Electrical Resistivity Tomography (Rücker et al., 2017). The inversion scheme employs a time-lapse approach following Karaoulis et al. (2014), minimizing an error-weighted objective function while incorporating both spatial and temporal smoothness constraints. Spatial regularization parameters of 80 and 15 were applied for Trench 1 and Trench 3, respectively, determined after several tests to reduce inversion artifacts and misfit. Temporal and spatial regularization parameter were set equal (scaling factor = 1), enforcing equal smoothness in both dimensions. The baseline resistivity model was used as the temporal reference, such that the inversion minimizes changes relative to initial conditions rather than between consecutive time steps. To account for remaining systematic uncertainties, a constant noise level of 2 % was incorporated into the inversion process. The misfit between modeled and observed data was evaluated using the relative root mean square error (RRMSE) and the chi-squared (χ^2) statistic (Rücker et al., 2006); χ^2 values ranged from 1 and 4 across all inversions.

https://doi.org/10.5194/egusphere-2026-4469
Preprint. Discussion started: 7 August 2026

The 2D inversions were performed on an unstructured triangular mesh that accounted for surface topography, with a minimum cell size at the surface of 0.1 m or 0.15 m, depending on the electrode distance. Temperature changes in Trench 1 during the sprinkling experiment did not exceed 1.5 °C in the first 10 cm and dropped below 1 °C at greater depths. In Trench 3, soil temperature changes were below 0.5 °C. Consequently, no temperature corrections were applied during data processing.

Variations in soil water content associated with the estimated bulk resistivity during the experiment were analyzed by calculating resistivity changes relative to the baseline values for each ERT profile. We defined three thresholds for resistivity decrease relative to baseline: 3 %, 5 %, and 10 %. These increases in electrical conductivity are reported as positive changes.

3 Results

3.1 SSF Flow Generation

As first described by Thoenes et al. (2026b), in Trench 1, the upper section had no flow before sprinkling and the lower section a steady 0.01 l s^{-1}. Both sections began responding about 30 minutes after sprinkling started (Figure 3a). Once the response began in the lower section, outflow continued to increase for the rest of the experiment, peaking 13 minutes after irrigation ceased at 0.33 l s^{-1}. The timing coincided with the SSF peak in the upper section. However, the upper section exhibited a two-phase rising limb: an initial, modest increase that was sustained until approximately two hours after irrigation began, followed by a steeper rise in outflow. After peaking, both sections entered a smooth recession phase. The lower section was still producing 0.08 l s^{-1} four hours after irrigation had ended. During the experiment, approx. 9200 l were applied and in the first 12 h after irrigation start, collected SSF volume was approx. 5200 l, yielding an event runoff coefficient of 0.57.

In Trench 3, with both sections starting without flow, a response in outflow was evident after 45 minutes in the bottom section and after 80 minutes in top (Figure 3b). Outflow then increased rapidly over a one-hour period before stagnating, though it continued to rise slightly, peaking precisely at the end of the irrigation phase. The maximum peak SSF outflow was approximately 0.45 l s^{-1} in the bottom section. After the peak, both sections exhibited recession: the top section ceased outflow after three hours, while the bottom section maintained an outflow of around 0.07 l s^{-1} four hours after irrigation ceased. In Trench 3, event runoff coefficient in the first 12 h after irrigation start was 0.61 with approx. 9000 l applied and 5500 l retrieved as SSF (Thoenes et al., 2026b).

3.2 Groundwater Level

At Trench 1, the groundwater levels prior to irrigation varied substantially between the wells (Figure 4-T1, see also Thoenes et al. (2026b)). A2 (located furthest uphill within the sprinkled area) exhibited the deepest initial water table at 1.53 meters below ground level (bgl) (see levels in Figure 6). Well A4 showed an intermediate level at approx. 0.70 m bgl, while A3 had the shallowest water table at 0.37 m bgl. During the first hour of irrigation, no clear response was observed in any of the wells. The initial reaction of A3 is uncertain due to a short data gap; however, once measurements resumed, the water table had risen by approximately 12 cm, suggesting that A3 likely responded not later than A2. Thereafter, A3 peaked at 0.16 m bgl. Well

https://doi.org/10.5194/egusphere-2026-4469
Preprint. Discussion started: 7 August 2026

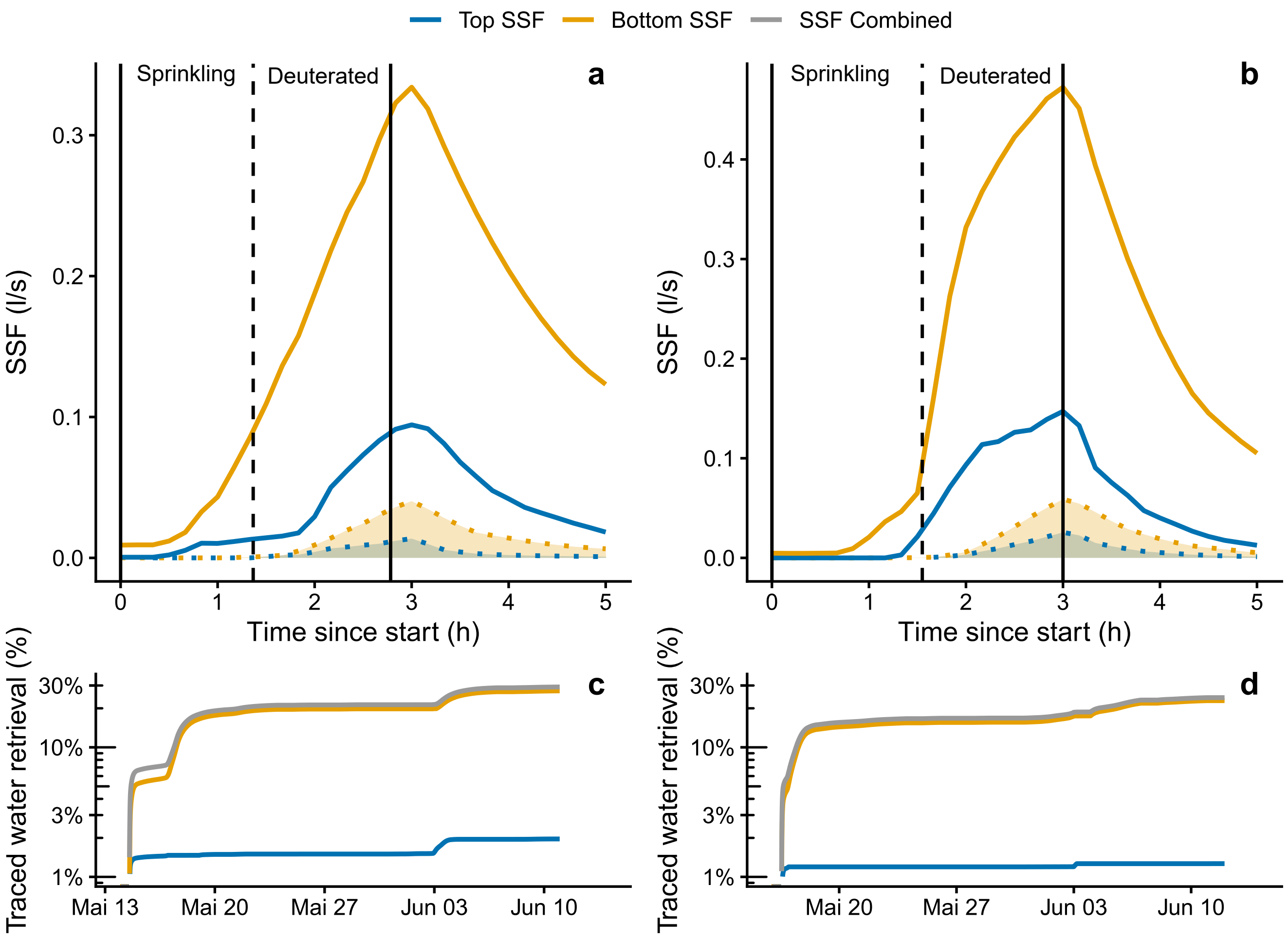

Figure 3. Trench 1 (a) and Trench 3 (b) SSF generation during the sprinkling experiment with recovered event water (dotted line with filled area) for each trench layer. Trench 1 (c) and Trench 3 (d) cumulative percentages of traced water retrieval over the next month after irrigation. Two large rainfall events occurred at the 18th of May (74 mm) and the 4th of June (63 mm).

https://doi.org/10.5194/egusphere-2026-4469
Preprint. Discussion started: 7 August 2026

A2 showed a gradual rise, reaching 1.03 m bgl and peaking at the end of the irrigation period. Well A4 displayed a similar response, peaking at the end of irrigation at 0.30 m bgl. Following the end of irrigation, the groundwater levels in all the wells declined.

At Trench 3, the initial groundwater pattern was reversed compared to Trench 1 (Figure 4-T3). Here A2 had a higher initial water table (0.78 m bgl) than A4 located close to the trench (1.25 m bgl) (see levels in Figure 7). Both wells responded to irrigation, but with distinct dynamics. Well A2 began to rise steadily after approximately one hour of irrigation, reaching a peak of 0.26 m bgl by the end of the sprinkling period. This was followed by a gradual recession. In contrast, A4 exhibited a delayed but sharp response: after around 1.5 hours, the water level increased abruptly by 100 cm over approximately 20 minutes, peaking at 0.20 m bgl by the end of the irrigation period. A slight recession followed thereafter. In both trenches, the groundwater level remained elevated for several hours after irrigation ceased, and did not return to its initial baseline within next 10 hours.

3.3 Isotopes

3.3.1 SSF Composition

Trench 1 exhibited a rapid response to the application of deuterated water. The upper section responded strongly within eight minutes (1 % tracer concentration in SSF), reaching a peak tracer concentration of 14.5 %. Following the end of irrigation, tracer contributions declined gradually to 5 %, where they remained stable. The lower section responded after 18 minutes (1 % tracer threshold), continuing to increase until the end of irrigation and peaking at 12.1 %. Thereafter, tracer concentrations in the lower section decreased to 5 % over the subsequent two hours. Of the 4800 l of deuterated water applied, 7.4 % was recovered (top 1.4 % and bottom 6.0 %) within the first 12 hours after tracer application start. Two subsequent natural rainfall events further mobilized traced water, resulting in a cumulative tracer recovery of 29 % over one month (Figure 3c, natural events 1 and 2 had 75 mm and 63 mm precipitation respectively).

The tracer response in Trench 3 was similar in magnitude to that in Trench 1. Tracer breakthrough occurred within seven minutes in the upper section and after 17 minutes in the lower section (1 % tracer threshold). Both sections peaked simultaneously at the end of the irrigation phase, reaching tracer contributions of 17.4 % and 12.5 % in the upper and lower sections, respectively. This was followed by a nearly parallel decline over the next two hours, with final concentrations of approximately 10 % (upper section) and 5 % (lower section). Within 12 hours after tracer application start, 11 % of the 4380 l of applied tracer water was recovered with 2.7 % from the upper section and 8.1 % from the lower section. Over the next month, a total of 32 % was recovered, primarily during the two major rainfall events that also triggered remobilization in Trench 1 (Figure 3d).

3.3.2 Soil Cores

One day after irrigation in Trench 1, the deuterated tracer was detected exclusively in the uppermost soil layers (0–10 cm and 10–20 cm). The top 10 cm samples were substantially enriched, although the isotopic signatures varied considerably between the three profiles, ranging from -30 ‰ to +15 ‰ δ^2H at 10 cm depth (Figure 5 a). One month later, the tracer signal in the

https://doi.org/10.5194/egusphere-2026-4469
Preprint. Discussion started: 7 August 2026

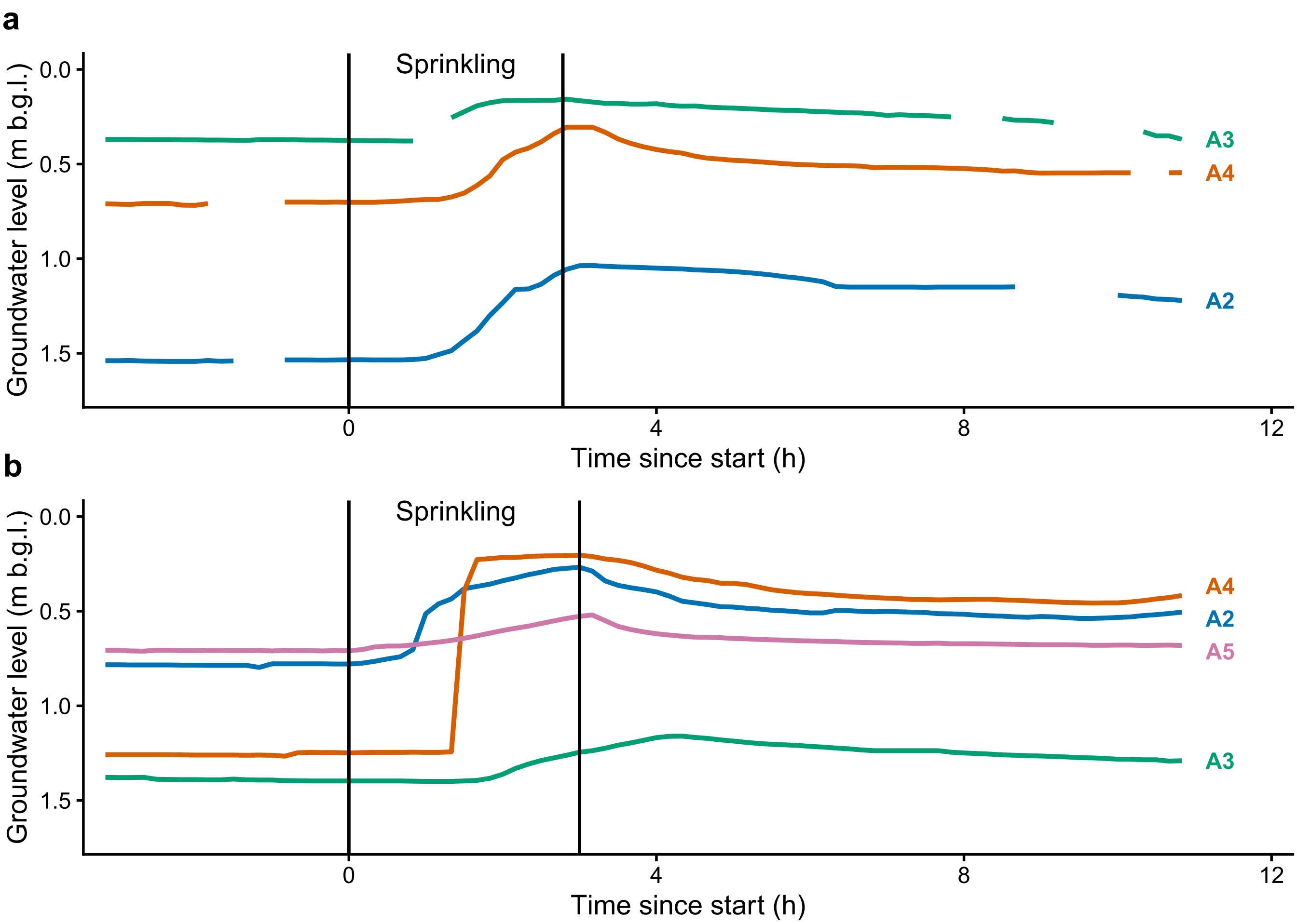

Figure 4. Groundwater level of the wells (Figure 2) within the sprinkling area for both trenches (**a** Trench 1; **b** Trench 3). Vertical lines indicate the duration of the sprinkling experiment.

topsoil had decreased to about -40 ‰ δ^2H (Figure 5). As a result from the mixing models, the mean volumetric tracer water content in the topsoil was 10 %. With an estimated available water volume of 22 m^3 in the first 20 cm over the 200 m^2 irrigated area (assuming saturation and a homogeneous porosity of 0.55), this corresponds to approximately 2.2 m^3 of traced water stored in the topsoil (around 45 % of traced water input). Notably, one of the three profiles showed a topsoil tracer contribution of 24 %, suggesting that actual storage may exceed this estimate.

3.4 ERT

At Trench 1, the baseline subsurface resistivity distribution across the irrigation area is shown for ERT profiles L1 and L3 in Figures 6a and f, respectively. In the L1 profile, the first 0.7 m of depth showed a lateral variation ranging from 80 to 700 Ωm. This variation is expected at these depths due to the presence of roots, bioturbation, and an abundance of cobble-sized clasts;

https://doi.org/10.5194/egusphere-2026-4469
Preprint. Discussion started: 7 August 2026

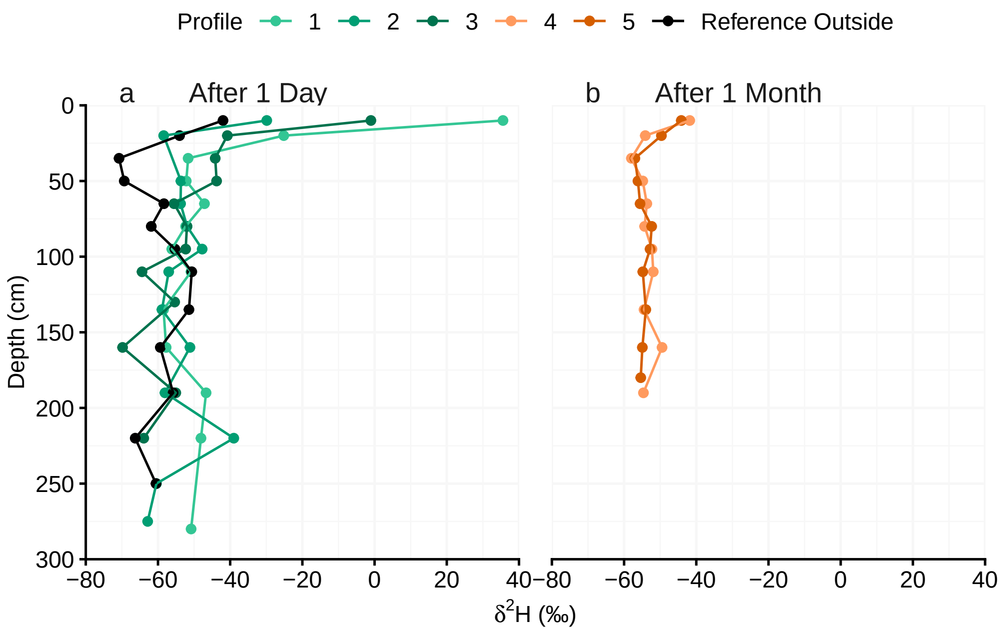

Figure 5. Pore water isotope profiles for δ^2H in the sprinkled area of Trench 1 **a** one day (green) and **b** 1 month (orange) after the irrigation experiment; the reference profile taken outside of the sprinkled area 1 day after irrigation is shown in black.

it is also consistent with the trench cut showing a high content of gravel and sandy material in a loamy matrix in the first 60 cm. Below this depth, the NE area showed resistivity values between 300 and 370 Ωm that decrease toward the SW to 100-200 Ωm. This low-resistivity zone is consistent with the grayish, reduced Gr horizon (a product of soil waterlogging (Smirnova and Kozlov, 2023)) on this side of the trench cut, which deepens to the NE of the trench.

In the L3 profile, the resistivity of the top heterogeneities in the first 0.5-0.6 m ranges between 100 and 700 Ωm. Below the top heterogeneities, most of the profile is dominated by a lower-resistivity layer, presumably consisting of a water-saturated matrix, with resistivity ranging from 100 to 200 Ωm. In the middle of the plot, a 4 m-wide area with higher resistivity (200-270 Ωm) extends vertically. The trench filling is characterized by the highest resistivity at this profile.

The relative resistivity changes with respect to the baseline distribution for ERT profiles L1 and L3 in Trench 1 are shown in Figure 6 b-e and g-j, respectively. The reduction in resistivity increased progressively over time, initially appearing in localized areas before expanding spatially. In L1, two areas showed more pronounced resistivity decreases: to the NE, a decrease of 9 % was detected after 1:18 h of sprinkling, which reached 13 % and 17 % at 2:22 and 3:35 h, respectively; to the SW, the maximum change reached 14 % and subsequently 18 %, maintaining this value until 3:35 h. After 23:27 h, a localized minimum of 15 % was observed, and the average resistivity change was around 8 %.

In L3, a maximum resistivity decrease was observed in the NW (downslope) section, where values decreased by 8 % after 44 minutes of sprinkling and continued to decline to 14 % and 22 % after 2 and 3 h, respectively; upslope, the response was

https://doi.org/10.5194/egusphere-2026-4469
Preprint. Discussion started: 7 August 2026

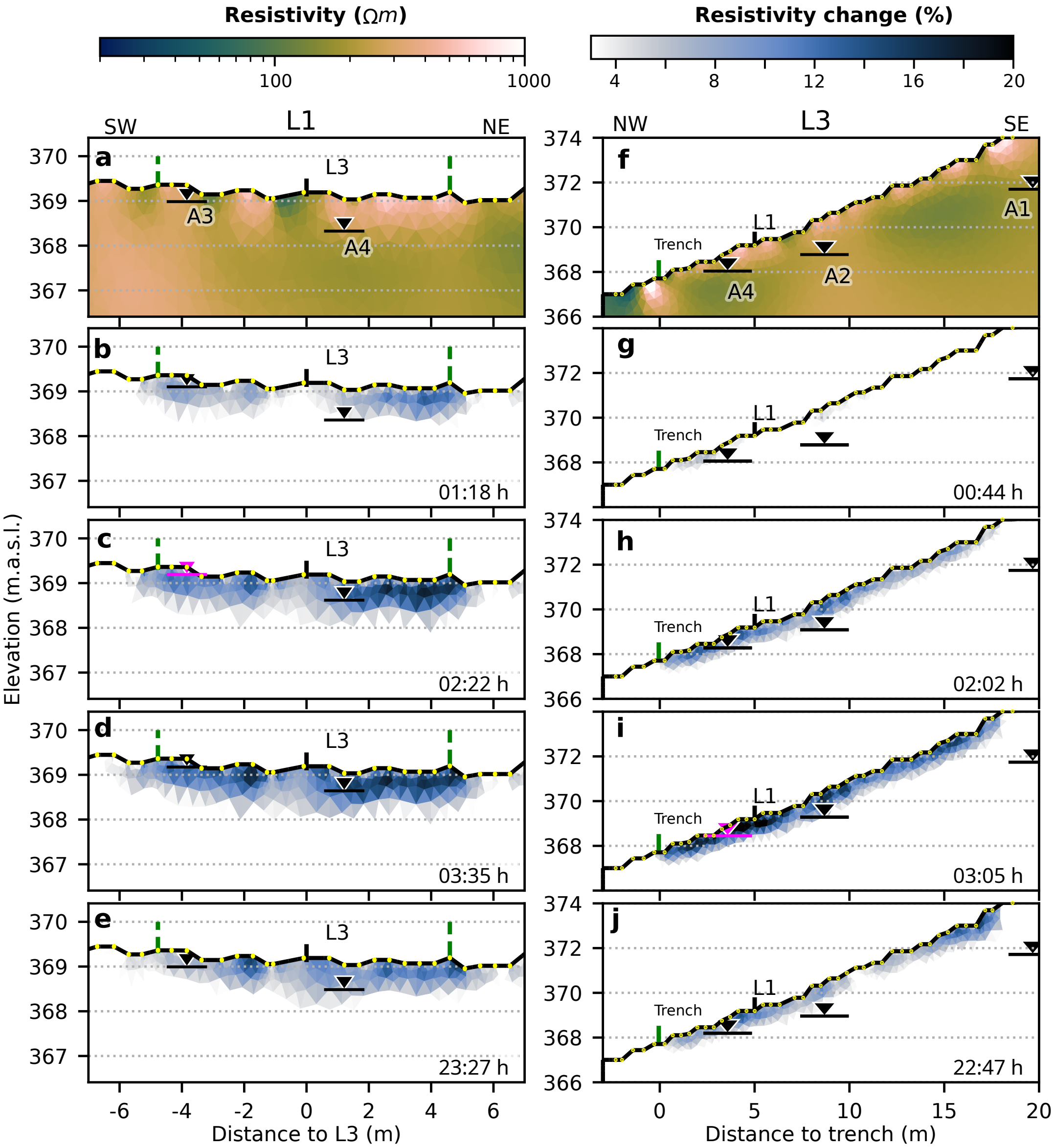

Figure 6. Trench 1 ERT results for profiles L1 and L3. Panels a-e correspond to profile L1 and show a zoomed-in view of the sprinkling area. Panel a presents the baseline bulk resistivity distribution, and panels b-e show the corresponding relative resistivity change, relative to the baseline resistivity model. Panels f-j correspond to profile L3 and display the full profile extent, with panel f showing the baseline bulk resistivity distribution and panels g-j show the corresponding relative resistivity change. Only resistivity decreases greater than 3 % relative to baseline resistivity are shown, and their values are plotted as positive. Green vertical lines represent the border of the sprinkling area. Times shown are relative to the start of sprinkling. Groundwater levels measured in monitoring wells are indicated by black and magenta lines in all panels; magenta is used where black lines would not be visible against the color scale.

https://doi.org/10.5194/egusphere-2026-4469
Preprint. Discussion started: 7 August 2026

slower, reaching 10 % after 2 h and peaking at 16 % in a small localized area, persisting for nearly 24 h. Beyond the 3 % resistivity change threshold, no substantial resistivity decrease persisted over the full 24 h; for comparability, this threshold was applied to both trenches. The zones with the largest resistivity decrease extended to 0.4–0.5 m depth.

The wetting front in L1, as determined by resistivity changes (limited to a minimum threshold of 3 %), after 01:18 h of irrigation, reached a depth of around 0.8 m towards the plot borders and 0.2 m in the center of the plot. This spatial distribution changed after the end of irrigation (3:35 h), reaching a depth of approximately 1 m in the center and NE and 0.7 m towards SW. At L3, the infiltration front deepened from around 0.5 m to 0.8 m in the lowest portion of the sprinkled area after 02:02 h, reaching a depth of around 0.9 m after the end of the irrigation (03:05 h).

The initial resistivity distribution at Trench 3 is shown in Figure 7a, Figure 7f, and Figure 7k, for lines L1, L2 and L3, respectively. In ERT L1, the top 0.5 m of soil exhibited resistivity values ranging from 200 to 3000 Ωm. The lowest values occurred at the lowest point of the profile topography, in a concave hillslope. The higher values were present to the NW of the plot area and extended to the extreme of the ERT profile. Below this 0.5-0.6 m depth, the resistivity values were mainly low, between 100 and 600 Ωm, presumably indicating a higher water content.

In the ERT profile L3, the top layer had resistivity values between 500 and 2000 Ωm. This higher-resistivity layer deepens towards the NE of the profile (upslope), reaching approximately 1.2 m depth at the end of the sprinkling plot. Below this higher-resistivity layer, resistivity values are generally low, around 200 Ωm in the upper part of the profile (upslope) and decreasing to approximately 100 Ωm downslope. At depths of 4 m, especially towards the NW (downslope), the resistivity starts to increase considerably; however, at these depths, we are close to the maximum ERT depth of investigation.

Relative resistivity changes with respect to baseline conditions for ERT profiles L1, L2, and L3 in Trench 3 are shown in Figure 7a–e, f–j, and k–o, respectively. During the first hour of sprinkling, small resistivity decreases appeared in localized areas. In L1, resistivity had decreased by up to 26 % at 00:56 h; the decrease then intensified to 32 % at 01:51 h and 35 % at 02:40 h, close to the end of irrigation. L2 showed resistivity changes of similar magnitude throughout irrigation, but with a different spatial distribution, showing the largest changes toward the SE, and reaching 35 % after 7 h, compared with 25 % in L1. In L3, resistivity had decreased by about 36 % at 01:25 h and reached a maximum decrease of 47 % in localized areas across the profile at 03:12 h. By 07:26 h the decrease had eased to 38 % near the trench and 30 % in the upper part of the sprinkling area. The zones with the largest resistivity decrease extended to 0.5–0.6 m depth.

The wetting front, determined from resistivity changes greater than 3 % at L1, extended to a depth of 1.2 m to the NW. In the remaining sprinkled area, the wetting front did not exceed 0.8 m throughout the entire experiment. At L2, the maximum depth after 7 hours was 1.6 m, located SE of the lower topography point. In the opposite direction, the wetting front was around 0.8 m deep during the final measurement. At L3, the infiltration front deepened from around 0.8 m to 1.7 m in the higher portion of the sprinkled area, with a smaller area near the trench reaching 1.1 m by the end of the sprinkling.

https://doi.org/10.5194/egusphere-2026-4469
Preprint. Discussion started: 7 August 2026

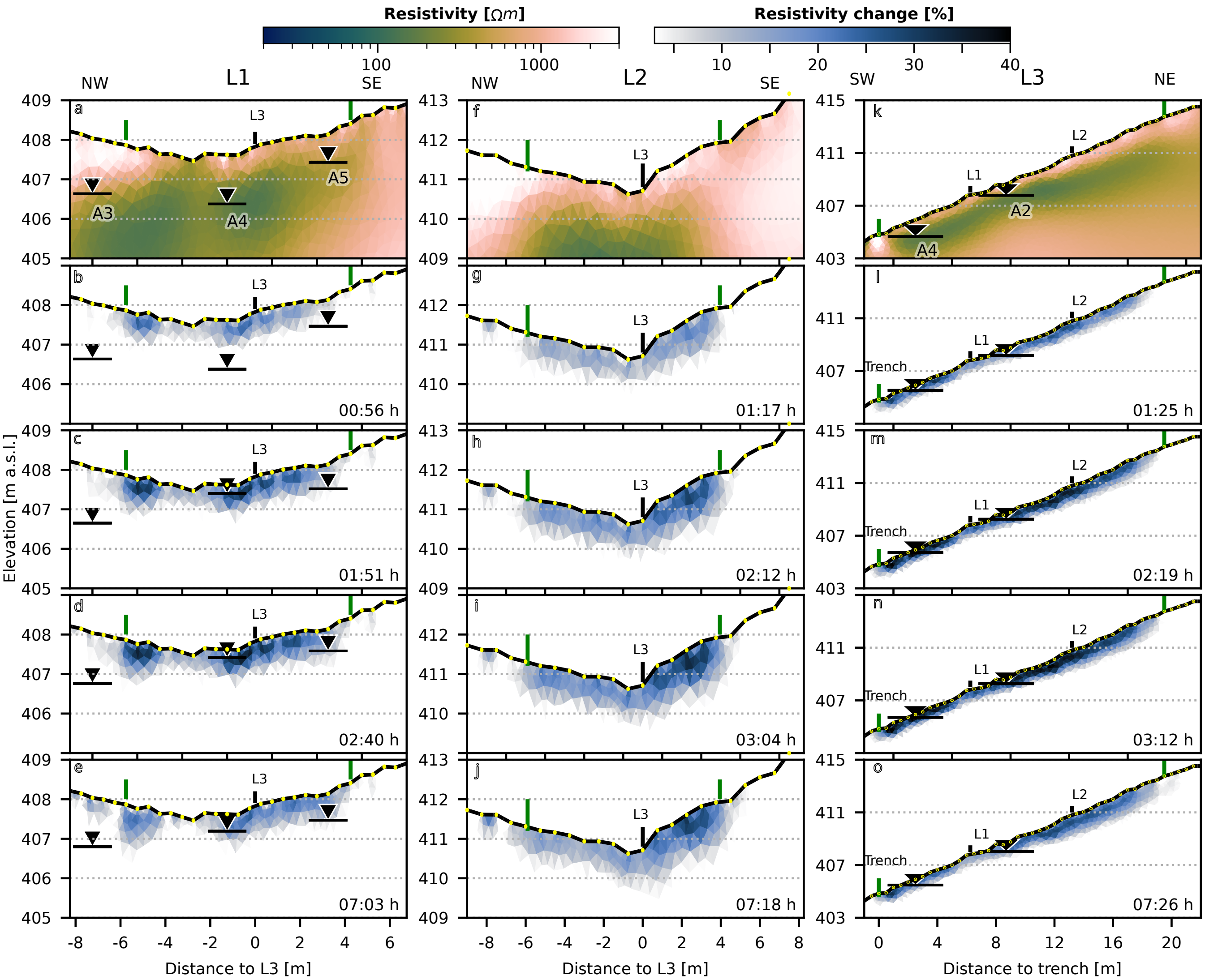

Figure 7. Trench 3 ERT results for profiles L1, L2 and L3. Panels a-e and panels f-j correspond to profile L1 and L2, respectively, and show a zoomed-in view with vertical exaggeration of the sprinkling area. Panel a and f present the baseline bulk resistivity distribution, and panels b-e and g-j show the corresponding relative resistivity change at different time steps, relative to the baseline resistivity model. Panels k-o correspond to profile L3 and display the full profile extent, with panel k showing the baseline bulk resistivity distribution and panels l-o the corresponding relative resistivity change. Green vertical lines represent the border of the sprinkling area. Displayed times are times since the start of sprinkling. Groundwater levels measured in monitoring wells are plotted on all panels.

https://doi.org/10.5194/egusphere-2026-4469
Preprint. Discussion started: 7 August 2026

4 Discussion

4.1 Outflow behavior

In Trench 1, flow responded in both depth sections at the same time, which points to initially unsaturated conditions near the top section. The rising limb of the upper section had two phases (Figure 3), suggesting that SSF dynamics at this shallower depth shifted after about 2 h toward a regime that favored lateral flow into the trench (Thoenes et al., 2026b). The GWL at A2 and A4, both on the central axis of the irrigation area, rose almost simultaneously after 1:20 h and reached 1.2 and 0.48 m bgl by 2 h (Figure 4). The water table therefore probably rose into a more permeable layer and fed more lateral flow to the upper section. ERT profile L3 supports this reading: the resistivity changes show that the wetting front reached the depth of the GWL at A4 after roughly 2 h of irrigation, and the accompanying resistivity decrease is independent evidence of increasing saturation in this zone. Because downward infiltration and the GWL rise occurred together, the ERT response likely reflects both processes.

In Trench 3, flow started in the bottom section, so SSF was triggered first at these depths. After 1.5 h, the SSF curve of this section steepened for about 30 min (Figure 3). The GWL at A4 rose abruptly at the same moment, and the GWLs in the other wells on the SE side (A2 and A5) had already been rising, so the steepening was probably a consequence of the rising water table. Within 2 h of sprinkling, the flow rate changed in both sections, first in the bottom one, and flow from the top section then held steadier over time. Water moving downslope or percolating deeper may have filled a different soil storage and drained laterally out of the irrigation area. The GWL in well A3, NW of and outside the irrigation perimeter, started rising at about the same time and marks this lateral movement. On this side of the area, the baseline ERT profiles L1 and L2 show a high-resistivity zone that decreased locally by up to 15 % during sprinkling, pointing to a change in water content there.

Across both study areas, the rise in groundwater level during sprinkling played a key role in controlling the SSF measured at each trench.

4.2 Dual Flow Domains

Results from both irrigation experiments indicate a dual-domain flow system. In this system, two coupled mechanisms govern the generation of lateral subsurface flow: preferential flow, which rapidly routes a fraction of event water through the soil profile, and piston flow, which mobilizes stored pre-event water.

The clearest evidence for preferential flow comes from the discrepancy between tracer depth and tracer distribution in the matrix. Deuterium appeared in both the top and bottom (> 70 cm bgl) trench sections within minutes of irrigation onset. However, post-irrigation soil cores detected deuterium only in the upper 20 cm of the soil matrix. Matrix flow alone cannot produce this pattern. If deuterated water had moved through the matrix to reach the lower trench section, measurable concentrations would have passed through the intervening soil. The absence of traced water below 20 cm in the matrix, combined with its substantial presence at depth in the outflow, suggests bypass flow through preferential pathways with little matrix interaction. The rapid decline in concentration once irrigation ceased, which receded faster than SSF outflow itself, reinforces this idea. The preferential pathways drained quickly once the hydraulic input stopped.

https://doi.org/10.5194/egusphere-2026-4469
Preprint. Discussion started: 7 August 2026

At the same time, the tracer budget revealed that preferential flow carried only a small fraction of the applied water. Traced water accounted for just 7–11 % of the traced sprinkled water volume on the day of irrigation. Meanwhile, soil sampling in Trench 1 confirmed that approximately 45 % of the tracer remained stored in the top 20 cm of the soil matrix. This is also supported by the still observable changes in resistivity after almost 24 h from the start of the sprinkling in most of the top soil of the ERT profiles. Although the outflow consisted mostly of unlabeled water, the runoff coefficient of 0.6 shows that the applied event water mobilized a large volume of stored pre-event water into SSF. These numbers together indicate that the dominant pathway for event water was infiltration into and temporary storage within the soil matrix. Outflow was not dominated by traced water, but rather by older, pre-event water displaced from the profile — a classic piston response.

The ERT and hydrometric data clarify the mechanism. During irrigation, the upper profile transitioned progressively from drier to wetter conditions, consistent with a wetting front advancing downward. The deeper zone, by contrast, remained near saturation throughout with negligible resistivity change, even though substantial lateral discharge was recorded in the lower trench. Outflow increased without any corresponding increase in storage at depth. This is the hydrometric signature of pressure-driven displacement: infiltrating water causes an increase of the hydraulic head, and a simultaneous increased forcing of vertical and lateral flow.

Long-term tracer recovery confirms that the matrix acts as both a sink and a delayed source. An additional 21 % of the applied tracer was released over the following month during two natural rainfall events. This demonstrates that a substantial portion of tracer was temporarily stored in the matrix rather than lost to deep percolation.

Taken together, these lines of evidence describe a system in which rapid preferential flow establishes the vertical hydraulic connection at depth while piston displacement of the saturated matrix delivers the bulk of the SSF response. The preferential pathways act as a fast conduit for a small volume of event water, and the matrix acts as a large reservoir whose stored water is mobilized by the pressure wave generated by infiltrating water.

Our observations align with prior studies on SSF dynamics and preferential flow behavior. The rapid trench response observed after irrigation is consistent with the finding that SSF can initiate quickly after a rainfall event, regardless of antecedent soil moisture conditions (Beasley, 1976). The high runoff coefficient (approx. 0.6) further supports the idea that SSF can account for a large proportion of up to 90 % of rainfall input in certain settings (Beasley, 1976). The isotopic composition of SSF quickly contained the signature of applied event water, suggesting the rapid activation of preferential flow paths. This agrees with studies showing that event water traveling through preferential pathways quickly contributes to SSF, bypassing the soil matrix (Freer et al., 2002; Kienzler and Naef, 2008; Anderson et al., 2009b; Beven and Germann, 2013; Angermann et al., 2017). Furthermore, labeled event water was detected in the bottom section trench but not found in the soil matrix in those depths. This finding further supports the existence of a connected preferential flowpath system that transports water vertically and laterally through the soil without interacting with the surrounding matrix, as was also observed by Gazis and Feng (2004); Anderson et al. (2009a, b); Peralta-Tapia et al. (2015); Angermann et al. (2017). Nevertheless, the majority of SSF collected during the sprinkling event consisted of unlabeled water. This "old water paradox" has been widely observed, and studies indicate that new event water displaces pre-event water, which then rapidly contributes to SSF (McDonnell, 1990; Anderson et al., 2009b; van Verseveld et al., 2017; Rinderer et al., 2021). In Trench 1, the continuous presence of labeled water in the upper

https://doi.org/10.5194/egusphere-2026-4469
Preprint. Discussion started: 7 August 2026

trench section after irrigation ceased suggests partial retention and mixing in the topsoil. This is consistent with the observation that macropore water eventually mixes with matrix water, yielding intermediate isotopic signatures over time (Leaney et al., 1993).

Overall, these findings support conceptualizing SSF as a dual-domain system involving rapid preferential flow and slower matrix flow, with the matrix not in equilibrium with the preferential flowpaths in terms of isotopic composition (Newman et al., 1998).

4.3 What Happened to the "Unaccounted" Labeled Water?

According to the retrieved tracer data, about 45 % of the labeled water remained stored in the topsoil matrix, and about 10 % was discharged during the first day of the sprinkling experiment. This leaves about 45 % of the traced water unaccounted for. Several plausible explanations exist:

Spatial Sampling Bias in Storage Estimation: If the soil profile with the highest observed tracer storage (24 %) is taken as representative and extrapolated across the entire 200 m^2 experimental plot, the resulting storage is 5.3 m^3, or 110 % of the applied tracer volume. This clearly overestimates the traced water, but it illustrates how little three soil cores (each 6 cm in diameter) can constrain a hillslope as heterogeneous as this one, where even the wetting patterns differ markedly across the plot (Figure 6). Porosity compounds the problem: it was measured at a single location and assumed uniform, yet a higher porosity from additional macropores or a lower one from a greater stone content would shift the available water volume in either direction. Taken together, these sampling limitations leave the storage in the upper soil layers poorly constrained, and the true value may be substantially higher than estimated — enough to account for a large share of the "missing" tracer.

Tracer Percolation and Deeper Lateral Flow: Within one month, approximately 30 % of the labeled water was captured in the trenches. Though small amounts of the traced water remained detectable in subsoil layers afterward, no additional tracer signal was observed in subsequent SSF samples. The residual tracer likely moved either downward into the bedrock beneath the depth of the trench. Bedrock can take up as much as 90 % of the percolating water (Tromp-van Meerveld et al., 2007). Much of this water then recharges groundwater, and only about 20 % feeds subsurface flow (Seiler et al., 2002) — close to what we measured here. Additionally, our trench installations were located on hillslopes with periglacial cover. The exact depth of the bedrock below those covers is uncertain. Lateral flow beneath the trench, especially at Trench 1, facilitated by these periglacial layers, is therefore plausible. These cover beds are known to influence SSF dynamics (Chifflard et al., 2008).

In conclusion, the "missing" tracer likely resulted from an underestimation of topsoil storage and from water pathways that bypassed trench capture, either through deep percolation into bedrock or through lateral flow beneath the depth of the trench. These processes are consistent with known hydrological behaviors in structured and heterogeneous hillslope systems.

4.4 Methodological Uncertainties

A key feature of our experimental design was that the isotopic signature of the initial sprinkling water matched that of the trench outflow. As a result unlabeled sprinkling water and pre-event water, could not be distinguished isotopically. The tracer experiment therefore isolated a single distinction: labeled versus unlabeled water. This design raises one concern. The large

https://doi.org/10.5194/egusphere-2026-4469
Preprint. Discussion started: 7 August 2026

volume of seemingly remobilized "old" water in the trench discharge might include unlabeled sprinkling water left over from the initial irrigation phase. We cannot rule this out entirely, but several lines of evidence point to most of that water being older water already stored in the hillslope. First, labeled water made up at most 14.5-17.8 % of peak flow. Had the earlier unlabeled sprinkling water traveled the same pathways, it would have reached the trench in comparable amounts. Second, core sampling revealed that most of the labeled water was retained in the topsoil. Since the experiment started with the application of unlabeled water to wet the soil matrix and reduce immediate tracer retention, it is likely that the initial (unlabeled) sprinkling water was also primarily retained in the topsoil rather than rapidly contributing to trench discharge.

A second source of uncertainty concerns the temporal resolution of our sampling. We collected samples every twenty minutes and then interpolated the results onto a ten-minute time frame. When we report that traced water appeared in SSF between those times, the tracer may in fact have reached the trench only at the moment of sampling rather than at some point beforehand. However, the interpolation remains reasonable, since the tracer concentration in the following samples shows a steady, continuous rise—which we also expect the intervening water to have taken.

Another uncertainty lies in the representativeness of the experimental rainfall conditions. Often studies investigating preferential flow rely on artificial sprinkling experiments with high intensity and volume (eg. Angermann et al. (2017) and Jackisch et al. (2017)). While these conditions are useful for triggering observable responses, they often exceed those of typical, moderate rainfall events. They may also activate preferential flow features that would remain inactive under natural conditions (Demand et al., 2019). With a sprinkling intensity of 15-16.6 mm/h, our study falls within this high-intensity range. This suggests that the observed activated flowpaths may not fully reflect those engaged during more frequent, moderate precipitation events.

A limitation of the time-lapse ERT method in this experiment concerns its sensitivity under saturated conditions. ERT sensitivity can decrease under overly wet soil conditions (Rao et al., 2020), an effect attributed either to data quality issues and spatial heterogeneity in the infiltration process (Wicki and Hauck, 2022), or to petrophysical insensitivity. Wu et al. (2023) showed in loess samples that once water content reaches the liquid limit, further increases no longer produce a marked decrease in resistivity. This is consistent with the behavior expected under near-full saturation, where pore spaces are already largely water-filled and additional water produces minimal contrast in the resistivity signal. As an additional limitation, the fresh water used as tracer in this study provides low resistivity contrast with the pre-existing pore water, further reducing the ability of ERT to detect active flow pathways. These combined effects must be considered when interpreting ERT-derived results in saturated or near-saturated zones, where the method may underestimate or entirely miss preferential flow paths.

Another limitation of the ERT method is its inability to resolve groundwater level behavior near the trench wall. The high resistivity of the trench filling material, combined with the survey geometry used in this study, produces inconclusive resistivity patterns in that zone. Since the trench wall acts as a sharp drainage face, the ERT results in its vicinity should be interpreted with caution.

The interpreted waterfront with a 3 % threshold was selected after testing higher values of 5 % and 10 %. At these higher thresholds, only small, localized changes remained visible 24 hours after the irrigation, and only the 3 % threshold captured a spatially consistent signal in Trench 1. While several authors adopt thresholds around 10 % (Vanella et al., 2021) and 5 %

https://doi.org/10.5194/egusphere-2026-4469
Preprint. Discussion started: 7 August 2026

(Clément et al., 2010), applying such a value to our data would have masked the decrease observed the day following the experiment, since most of the resistivity changes fell below the 10 % level. A lower threshold was therefore justified in our case since it preserved sensitivity to the response we sought to characterize, whereas a more conservative cut-off would have suppressed a physically meaningful feature of our data.

5 Conclusions

We conducted a combined deuterium-labeled sprinkling experiment and time-lapse ERT, alongside groundwater observations and soil water isotope profiling, to investigate the contribution of event water to SSF, the dominant flow paths, and the joint characterization of subsurface flow dynamics using tracer and geophysical methods on two forested hillslopes.

Our results demonstrate that SSF at both sites is governed by a dual-domain system of coupled fast and slow flow mechanisms. Event water reached the trenches within minutes of tracer application, even at depths below 70 cm. Meanwhile, it remained undetectable in the soil matrix below 20 cm, providing evidence of connected preferential pathways that transmit water vertically and laterally with minimal matrix interaction. The majority of the SSF response consisted of unlabeled water displaced from the deeper, near-saturated profile. Due to this saturation, ERT recorded negligible resistivity change in this area despite substantial lateral discharge. This suggests piston-type, pressure-driven displacement rather than the transfer of new water. Around 45 % of the labeled water was stored in the topsoil, acting as a reservoir that was partially remobilized during subsequent natural rainfall events. This increased cumulative tracer recovery to around 30 % within one month. The remaining unaccounted tracer most plausibly reflects underestimated topsoil storage, as well as flow paths that bypass the trenches via deep percolation or lateral flow beneath the trench installation depth.

Methodologically, the two approaches were complementary: isotopes quantified the sources and the small event-water fraction of SSF, while ERT identified the spatial and temporal patterns of resistivity change associated with the advancing wetting front. A promising next step would be to use multiple tracers together that can be detected by both isotopic and geoelectrical methods simultaneously. An adequately conductive tracer could enable ERT to directly image the distribution of flow paths, including within the saturated zone where fresh-water infiltration currently produces no resistivity contrast.

https://doi.org/10.5194/egusphere-2026-4469
Preprint. Discussion started: 7 August 2026

Appendix A

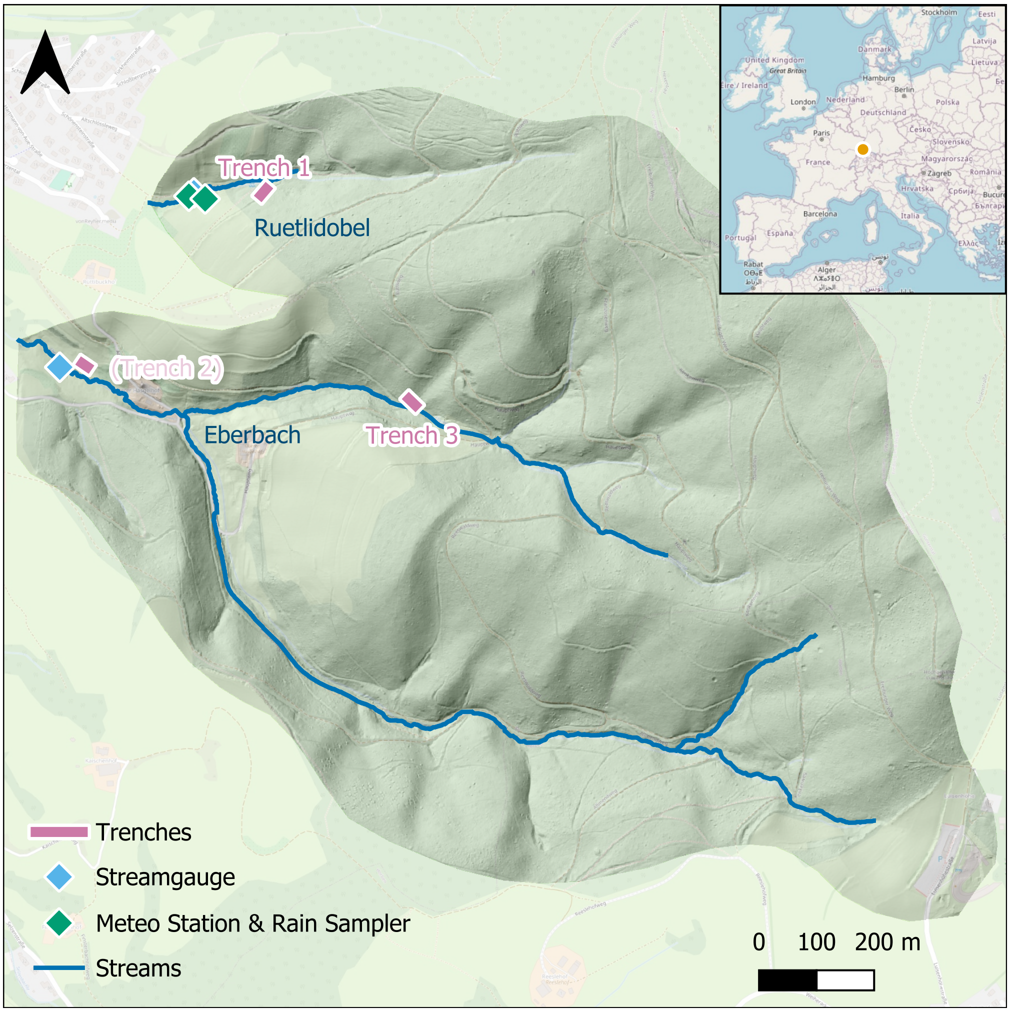

Figure A1. Map of the research catchment, produced by the authors with data from OpenStreetMap contributors (2017)

Data availability. The used tracer and trenchflow datasets are available in the SSF Research Units own public Data Warehouse accessible at https://vhrz669.hrz.uni-marburg.de/ssf/data_pre.do?cmd=showall. The ERT Data can be found in the supplementary material.

Author contributions. All authors designed the experiment. JP, VC, JW, ET and VL conducted the field measurements. JP, VC and JW wrote the first draft. All authors revised and approved the final manuscript. SH, MW, SA and BK secured the funding for the study

Competing interests. At least one of the (co-)authors is a member of the editorial board of Hydrology and Earth System Sciences.

Acknowledgements. We want to thank all the technicians and people involved in fieldwork without whom it would have been impossible to perform the sprinkling experiments (Martin Kügel, Sören Köhler, Yvonne Schadewell). This research has been supported by the Deutsche Forschungsgemeinschaft (project no. 453746323) through the research unit FOR 5288: "Fast and Invisible: Conquering Subsurface Stormflow through an Interdisciplinary Multi-Site Approach".

https://doi.org/10.5194/egusphere-2026-4469
Preprint. Discussion started: 7 August 2026

References

Allen, S. T., Keim, R. F., and McDonnell, J. J.: Spatial Patterns of Throughfall Isotopic Composition at the Event and Seasonal Timescales, Journal of Hydrology, 522, 58–66, https://doi.org/10.1016/j.jhydrol.2014.12.029, 2015.

Anderson, A. E., Weiler, M., Alila, Y., and Hudson, R. O.: Dye Staining and Excavation of a Lateral Preferential Flow Network, Hydrology and Earth System Sciences, 13, 935–944, https://doi.org/10.5194/hess-13-935-2009, 2009a.

Anderson, A. E., Weiler, M., Alila, Y., and Hudson, R. O.: Subsurface Flow Velocities in a Hillslope with Lateral Preferential Flow: HILLSLOPE PREFERENTIAL FLOW VELOCITIES, Water Resources Research, 45, https://doi.org/10.1029/2008WR007121, 2009b.

Angermann, L., Jackisch, C., Allroggen, N., Sprenger, M., Zehe, E., Tronicke, J., Weiler, M., and Blume, T.: Form and Function in Hillslope Hydrology: Characterization of Subsurface Flow Based on Response Observations, Hydrology and Earth System Sciences, 21, 3727–3748, https://doi.org/10.5194/hess-21-3727-2017, 2017.

Bachmair, S. and Weiler, M.: Hillslope Characteristics as Controls of Subsurface Flow Variability, Hydrology and Earth System Sciences, 16, 3699–3715, https://doi.org/10.5194/hess-16-3699-2012, 2012.

Beasley, R. S.: Contribution of Subsurface Flow from the Upper Slopes of Forested Watersheds to Channel Flow, Soil Science Society of America Journal, 40, 955–957, https://doi.org/10.2136/sssaj1976.03615995004000060039x, 1976.

Beven, K. and Germann, P.: Macropores and Water Flow in Soils Revisited: REVIEW, Water Resources Research, 49, 3071–3092, https://doi.org/10.1002/wrcr.20156, 2013.

Brodersen, C., Pohl, S., Lindenlaub, M., Leibundgut, C., and v Wilpert, K.: Influence of Vegetation Structure on Isotope Content of Throughfall and Soil Water, Hydrological Processes, 14, 1439–1448, https://doi.org/10.1002/1099-1085(20000615)14:8<1439::AID-HYP985>3.0.CO;2-3, 2000.

Chifflard, P., Didszun, J., and Zepp, H.: Skalenübergreifende Prozess-Studien zur Abflussbildung in Gebieten mit periglazialen Deckschichten (Sauerland, Deutschland), Grundwasser, 13, 27–41, https://doi.org/10.1007/s00767-007-0058-1, 2008.

Chifflard, P., Blume, T., Maerker, K., Hopp, L., Van Meerveld, I., Graef, T., Gronz, O., Hartmann, A., Kohl, B., Martini, E., Reinhardt-Imjela, C., Reiss, M., Rinderer, M., and Achleitner, S.: How Can We Model Subsurface Stormflow at the Catchment Scale If We Cannot Measure It?, Hydrological Processes, 33, 1378–1385, https://doi.org/10.1002/hyp.13407, 2019.

Clément, R., Descloitres, M., Günther, T., Oxarango, L., Morra, C., Laurent, J.-P., and Gourc, J.-P.: Improvement of Electrical Resistivity Tomography for Leachate Injection Monitoring, 30, 452–464, https://doi.org/10.1016/j.wasman.2009.10.002, 2010.

Craig, H.: Isotopic Variations in Meteoric Waters, Science, 133, 1702–1703, https://doi.org/10.1126/science.133.3465.1702, 1961.

Demand, D., Blume, T., and Weiler, M.: Spatio-Temporal Relevance and Controls of Preferential Flow at the Landscape Scale, Hydrology and Earth System Sciences, 23, 4869–4889, https://doi.org/10.5194/hess-23-4869-2019, 2019.

Freer, J., McDonnell, J. J., Beven, K. J., Peters, N. E., Burns, D. A., Hooper, R. P., Aulenbach, B., and Kendall, C.: The Role of Bedrock Topography on Subsurface Storm Flow: THE ROLE OF BEDROCK TOPOGRAPHY ON SUBSURFACE STORM FLOW, Water Resources Research, 38, 5–1–5–16, https://doi.org/10.1029/2001WR000872, 2002.

Fujimoto, M., Ohte, N., and Tani, M.: Effects of Hillslope Topography on Runoff Response in a Small Catchment in the Fudoji Experimental Watershed, Central Japan, Hydrological Processes, 25, 1874–1886, https://doi.org/10.1002/hyp.7943, 2011.

Gazis, C. and Feng, X.: A Stable Isotope Study of Soil Water: Evidence for Mixing and Preferential Flow Paths, Geoderma, 119, 97–111, https://doi.org/10.1016/S0016-7061(03)00243-X, 2004.

Govan, E. and Parnell, A.: Simmr: A Stable Isotope Mixing Model, 2023.

https://doi.org/10.5194/egusphere-2026-4469
Preprint. Discussion started: 7 August 2026

Guo, L., Chen, J., and Lin, H.: Subsurface Lateral Preferential Flow Network Revealed by Time-Lapse Ground-Penetrating Radar in a Hillslope, Water Resources Research, 50, 9127–9147, https://doi.org/10.1002/2013WR014603, 2014.

Hopp, L. and McDonnell, J.: Connectivity at the Hillslope Scale: Identifying Interactions between Storm Size, Bedrock Permeability, Slope Angle and Soil Depth, Journal of Hydrology, 376, 378–391, https://doi.org/10.1016/j.jhydrol.2009.07.047, 2009.

Jackisch, C., Angermann, L., Allroggen, N., Sprenger, M., Blume, T., Tronicke, J., and Zehe, E.: Form and Function in Hillslope Hydrology: In Situ Imaging and Characterization of Flow-Relevant Structures, Hydrology and Earth System Sciences, 21, 3749–3775, https://doi.org/10.5194/hess-21-3749-2017, 2017.

Karaoulis, M., Tsourlos, P., Kim, J.-H., and Revil, A.: 4D Time-lapse ERT Inversion: Introducing Combined Time and Space Constraints, Near Surface Geophysics, 12, 25–34, https://doi.org/10.3997/1873-0604.2013004, 2014.

Kato, H., Onda, Y., Nanko, K., Gomi, T., Yamanaka, T., and Kawaguchi, S.: Effect of Canopy Interception on Spatial Variability and Isotopic Composition of Throughfall in Japanese Cypress Plantations, Journal of Hydrology, 504, 1–11, https://doi.org/10.1016/j.jhydrol.2013.09.028, 2013.

Kelln, C., Barbour, L., and Qualizza, C.: Preferential Flow in a Reclamation Cover: Hydrological and Geochemical Response, Journal of Geotechnical and Geoenvironmental Engineering, 133, 1277–1289, https://doi.org/10.1061/(ASCE)1090-0241(2007)133:10(1277), 2007.

Kienzler, P. M. and Naef, F.: Subsurface Storm Flow Formation at Different Hillslopes and Implications for the 'Old Water Paradox', Hydrological Processes, 22, 104–116, https://doi.org/10.1002/hyp.6687, 2008.

Koch, K. M.: Application of Electrical Resistivity Tomography (ERT) Together with Tracer Data to Identify Hydrological Process Areas at a Surface Water / Groundwater Test Site, 2004.

Leaney, F. W., Smettem, K. R. J., and Chittleborough, D. J.: Estimating the Contribution of Preferential Flow to Subsurface Runoff from a Hillslope Using Deuterium and Chloride, Journal of Hydrology, 147, 83–103, https://doi.org/10.1016/0022-1694(93)90076-L, 1993.

Leslie, I. and Heinse, R.: Characterizing Soil–Pipe Networks with Pseudo-Three-Dimensional Resistivity Tomography on Forested Hillslopes with Restrictive Horizons, Vadose Zone Journal, 12, vzj2012.0200, https://doi.org/10.2136/vzj2012.0200, 2013.

LGL BW: Digitale Geländemodelle, https://www.lgl-bw.de/Produkte/3D-Produkte/Digitale-Gelaendemodelle/, 2026.

McDonnell, J. J.: A Rationale for Old Water Discharge Through Macropores in a Steep, Humid Catchment, Water Resources Research, 26, 2821–2832, https://doi.org/10.1029/WR026i011p02821, 1990.

McGuire, K. J., Klaus, J., and Jackson, C. R.: Interflow, Subsurface Stormflow and Throughflow: A Synthesis of Field Work and Modelling, Hydrological Processes, 38, e15 263, https://doi.org/10.1002/hyp.15263, 2024.

McMillan, H., Araki, R., Bolotin, L., Kim, D.-H., Coxon, G., Clark, M., and Seibert, J.: Global Patterns in Observed Hydrologic Processes, Nature Water, pp. 1–10, https://doi.org/10.1038/s44221-025-00407-w, 2025.

Newman, B. D., Campbell, A. R., and Wilcox, B. P.: Lateral Subsurface Flow Pathways in a Semiarid Ponderosa Pine Hillslope, Water Resources Research, 34, 3485–3496, https://doi.org/10.1029/98WR02684, 1998.

OpenStreetMap contributors: Planet dump retrieved from https://planet.osm.org , https://www.openstreetmap.org, 2017.

Peralta-Tapia, A., Sponseller, R. A., Tetzlaff, D., Soulsby, C., and Laudon, H.: Connecting Precipitation Inputs and Soil Flow Pathways to Stream Water in Contrasting Boreal Catchments, Hydrological Processes, 29, 3546–3555, https://doi.org/10.1002/hyp.10300, 2015.

Pyschik, J., Kuleshov, A., Fasching, C., Chifflard, P., Hopp, L., Blume, T., and Weiler, M.: A Comparative Study of Subsurface Stormflow at Three Trenched Hillslopes: Sources, Pathways and Tracer Behaviour, https://doi.org/10.22541/essoar.174922649.90488517/v1, 2025a.

Pyschik, J., Seeger, S., Herbstritt, B., and Weiler, M.: Technical Note: A Fast and Reproducible Autosampler for Direct Vapor Equilibration Isotope Measurements, Hydrology and Earth System Sciences, 29, 525–534, https://doi.org/10.5194/hess-29-525-2025, 2025b.

Rao, S., Lesparre, N., Flores-Orozco, A., Wagner, F., Kemna, A., and Javaux, M.: Imaging Plant Responses to Water Deficit Using Electrical Resistivity Tomography, 454, 261–281, https://doi.org/10.1007/s11104-020-04653-7, 2020.

Rinderer, M., Krüger, J., Lang, F., Puhlmann, H., and Weiler, M.: Subsurface Flow and Phosphorus Dynamics in Beech Forest Hillslopes during Sprinkling Experiments: How Fast Is Phosphorus Replenished?, Biogeosciences, 18, 1009–1027, https://doi.org/10.5194/bg-18-1009-2021, 2021.

Rücker, C., Günther, T., and Spitzer, K.: Three-Dimensional Modelling and Inversion of Dc Resistivity Data Incorporating Topography - I. Modelling, Geophysical Journal International, 166, 495–505, https://doi.org/10.1111/j.1365-246X.2006.03010.x, 2006.

Rücker, C., Günther, T., and Wagner, F. M.: pyGIMLi: An Open-Source Library for Modelling and Inversion in Geophysics, Computers & Geosciences, 109, 106–123, https://doi.org/10.1016/j.cageo.2017.07.011, 2017.

Scaini, A., Audebert, M., Hissler, C., Fenicia, F., Gourdol, L., Pfister, L., and Beven, K. J.: Velocity and Celerity Dynamics at Plot Scale Inferred from Artificial Tracing Experiments and Time-Lapse ERT, Journal of Hydrology, 546, 28–43, https://doi.org/10.1016/j.jhydrol.2016.12.035, 2017.

Seiler, K. P., von Loewenstern, S., and Schneider, S.: Matrix and Bypass-Flow in Quaternary and Tertiary Sediments of Agricultural Areas in South Germany, Geoderma, 105, 299–306, https://doi.org/10.1016/S0016-7061(01)00109-4, 2002.

Smirnova, M. A. and Kozlov, D. N.: Soil Properties as Indicators of Soil Water Regime: A Review, Eurasian Soil Science, 56, 306–320, https://doi.org/10.1134/S1064229322602396, 2023.

Sponagel, H., Eckelmann, W., Ad-hoc-Arbeitsgruppe Boden der Staatlichen Geologischen Dienste und der Bundesanstalt für Geowissenschaften und Rohstoffe, and Bundesanstalt für Geowissenschaften und Rohstoffe, eds.: Bodenkundliche Kartieranleitung: mit 41 Abbildungen, 103 Tabellen und 31 Listen, Bundesanst. für Geowiss. und Rohstoffe, Hannover, 5., verbesserte und erweiterte auflage edn., ISBN 978-3-510-95920-4 978-3-510-95804-7, 2005.

Thoenes, E., Blume, T., Weiler, M., Kohl, B., Hopp, L., and Achleitner, S.: Influence of Rainfall Event Characteristics and Antecedent Conditions on Subsurface Stormflow Response of Two Forested Hillslopes, Hydrology and Earth System Sciences, 30, 4405–4436, https://doi.org/10.5194/hess-30-4405-2026, 2026a.

Thoenes, E., Pyschik, J., Weiler, M., Lechner, V., Kohl, B., and Achleitner, S.: Exploring Subsurface Stormflow through Sprinkling Experiments at Multiple Trenchsites, ESS Open Archive, 2026, https://doi.org/10.22541/essoar.15006118/v1, 2026b.

Tromp-van Meerveld, H. J. and McDonnell, J. J.: Threshold Relations in Subsurface Stormflow: 2. The Fill and Spill Hypothesis: THRESHOLD FLOW RELATIONS, 2, Water Resources Research, 42, https://doi.org/10.1029/2004WR003800, 2006.

Tromp-van Meerveld, H. J., Peters, N. E., and McDonnell, J. J.: Effect of Bedrock Permeability on Subsurface Stormflow and the Water Balance of a Trenched Hillslope at the Panola Mountain Research Watershed, Georgia, USA, Hydrological Processes, 21, 750–769, https://doi.org/10.1002/hyp.6265, 2007.

Uhlenbrook, S. and Wenninger, J.: Identification of Flow Pathways along Hillslopes Using Electrical Resistivity Tomography (ERT), 2006.

van Verseveld, W. J., Barnard, H. R., Graham, C. B., McDonnell, J. J., Brooks, J. R., and Weiler, M.: A Sprinkling Experiment to Quantify Celerity–Velocity Differences at the Hillslope Scale, Hydrology and Earth System Sciences, 21, 5891–5910, https://doi.org/10.5194/hess-21-5891-2017, 2017.

Vanella, D., Ramírez-Cuesta, J. M., Sacco, A., Longo-Minnolo, G., Cirelli, G. L., and Consoli, S.: Electrical Resistivity Imaging for Monitoring Soil Water Motion Patterns under Different Drip Irrigation Scenarios, 39, 145–157, https://doi.org/10.1007/s00271-020-00699-8, 2021.

https://doi.org/10.5194/egusphere-2026-4469
Preprint. Discussion started: 7 August 2026

605 Weiler, M., McDonnell, J. J., Tromp-van Meerveld, I., and Uchida, T.: Subsurface Stormflow, in: Encyclopedia of Hydrological Sciences, edited by Anderson, M. G. and McDonnell, J. J., p. hsa119, John Wiley & Sons, Ltd, Chichester, UK, ISBN 978-0-471-49103-3 978-0-470-84894-4, https://doi.org/10.1002/0470848944.hsa119, 2005.

Wicki, A. and Hauck, C.: Monitoring Critically Saturated Conditions for Shallow Landslide Occurrence Using Electrical Resistivity Tomography, 21, e20 204, https://doi.org/10.1002/vzj2.20204, 2022.

610 Wilson, G. V., Rigby, J. R., Ursic, M., and Dabney, S. M.: Soil Pipe Flow Tracer Experiments: 1. Connectivity and Transport Characteristics, Hydrological Processes, 30, 1265–1279, https://doi.org/10.1002/hyp.10713, 2016.

Wu, J., Dai, F., Liu, P., Huang, Z., and Meng, L.: Application of the Electrical Resistivity Tomography in Groundwater Detection on Loess Plateau, 13, 4821, https://doi.org/10.1038/s41598-023-31952-7, 2023.